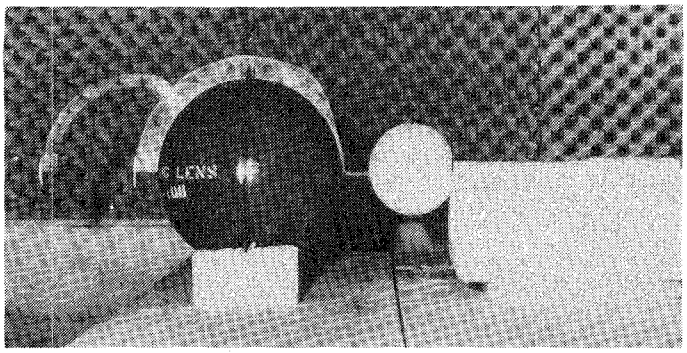

Fig. 5. Apparatus for electric field measurement behind a dielectric lens.

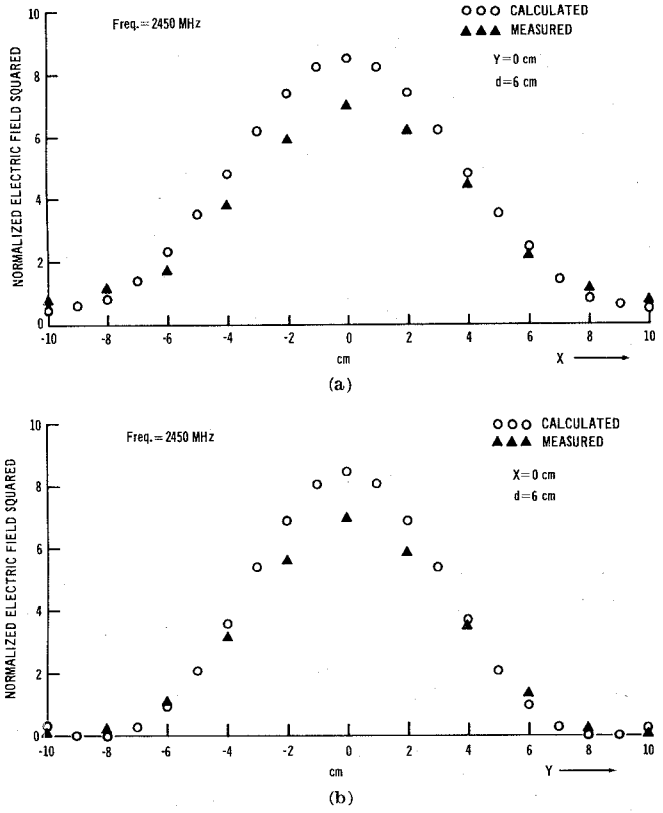

Fig. 6. Comparison of calculated and measured normalized electric field squared in a 20-cm × 20-cm X–Y plane, 6 cm behind a polyfoam sphere. (a) Along the direction of incident electric field vector (E_0). (b) Along the direction of incident magnetic-field vector (H_0).

comparison to that of incident magnetic field direction as is predicted by the calculation. The slightly lower measured peak compared to the calculated value is expected from the averaging effect of the measuring antenna which has a 5-cm diameter.

DISCUSSION

The results of the investigation indicate that the focusing effect of dielectric spheres depends on dielectric material, sphere size, and source frequency. The Stycast 35 DA dielectric material which has a relative dielectric constant of 5.0 does not perform as well as polyethylene ($\epsilon' = 2.26$) and polyfoam ($\epsilon' = 1.89$) in focusing electric fields. Hence the approach of increasing the dielectric constant in hope of increasing focusing of radiation may not be valid. The electric field may be focused internally in the sphere with $\epsilon' = 5.0$. The increase of focusing factor with increased sphere diameter is found. However, the increase is not monotonic. The source frequency affects both beamwidth of focused radiation and its peak. The result indicates that the source frequency is the primary controlling factor of the width of the base of the focused beam. However, for a highly focused beam, the value of the electric field squared at the base of the beam will be very small compared to that of the peak. For the practical applications of selective exposure, one may define a beam spot to be the region across which the focused electric field squared attenuates from its peak value to a given fraction of the peak value, such as one-tenth. The beam spot is therefore dependent on the focusing factor as well as the source frequency. Hence, the peak and the beam spot of the focused beam can be partially controlled by the magnitude of incident power density and the sphere diameter without changing source frequency.

CONCLUSION

This investigation indicates that by proper selection of source frequency, dielectric materials, and the size of the dielectric spheres, specified focused microwave radiation can be produced for localized exposure of biological subjects. This technique may also be useful for medical applications such as noncontact selective heating of diseased tissues as an alternative to surgical removal, the therapeutic selective heating of wounded tissues, and selective heating in conjunction with chemotherapy.

It should be emphasized that the electric fields calculated and measured in this investigation are exposure fields in the absence of the subject to be irradiated. It is expected that the presence of the irradiated object near this exposure field will significantly alter the exposure field. Also, the tissue penetration characteristics of such a focused microwave exposure field is as yet not determined. The significant dependence of microwave absorption patterns in tissues due to different sources (exposure fields) has been reported [5]. Additional work is needed to determine the tissue absorption characteristics of the focused exposure field. In the current investigation, the apparatus for producing a focused exposure field requires a plane-wave source and hence an anechoic chamber as well as a high-power generator. To increase the practical utility of the dielectric sphere, research may be needed to determine the possibility of replacing the incident plane-wave source with a more practical source.

REFERENCES

[1] R. L. Carpenter, E. S. Ferri, and G. J. Hagan, "Use of a dielectric lens for experimental microwave irradiation of the eye," presented at the 1974 Conf. Biological Effects of Non-ionizing Radiation, Academy of Sciences, New York, Feb. 12–15, 1974.
[2] T. C. Chestan and E. I. Luma "Constant-K lenses," in *ALP Tech. Dig.*, Mar.–Apr. 1963.
[3] G. Bekefi and G. W. Farnell, "A homogeneous dielectric sphere as a microwave lens," *Can. J. Phys.*, vol. 34, pp. 790–803, 1956.
[4] J. A. Stratton, *Electromagnetic Theory*. New York: McGraw-Hill, 1941, pp. 563–570.
[5] H. S. Ho, "Contrast of dose distribution in phantom heads due to aperture and plane wave sources," *Ann. N. Y. Acad. Sci.*, vol. 247, pp. 454–472, 1975.

On the Synthesis of Waveguides and Cavities Realized with Nonseparable Solutions of Helmholtz Wave Equation

P. J. LUYPAERT AND D. H. SCHOONAERT

***Abstract*—This short paper shows how nonseparable solutions of the Helmholtz wave equation can be used in the synthesis of waveguides and cavities with nonconventional cross section, and also investigates the attenuation and Q factor.**

Manuscript received March 17, 1975; revised July 21, 1975.
The authors are with the Department of Electronics, Catholic University of Louvain, Heverleer, Louvain, Belgium.

INTRODUCTION

Simple nonseparable solutions of the Helmholtz wave equation are occasionaly mentioned in the literature [1]. Moseley discovered a whole class of nonseparable solutions through the use of a generative differential operator as shown in [2]. Further we have analyzed [3] the use of cavities, synthesized with nonseparable solutions of the Helmholtz wave equation. It is the aim of this study to use nonseparable solutions in the synthesis of waveguides and cavities and to investigate some interesting properties.

ANALYSIS

Let

$$\nabla^2\phi(x,y) + k^2\phi(x,y) = 0 \tag{1}$$

be the Helmholtz wave equation for a two-dimensional case. The separable solution will be given by:

$$\phi^{(0)}(x,y) = \sin(\alpha x + \beta)\sin(\gamma y + \delta) \tag{2}$$

with

$$\alpha^2 + \gamma^2 = k^2. \tag{3}$$

If we form a two-dimensional operator

$$\mathrm{H} = \gamma\frac{\partial}{\partial\alpha} - \alpha\frac{\partial}{\partial\gamma} \tag{4}$$

and operate upon the function $\phi^{(0)}(xy)$, we obtain a nonseparable solution which is also a solution of (1). After iterative use of H we find a series of nonseparable solutions $\phi^{(1)}(xy), \phi^{(2)}(xy) \cdots \phi^{(n)}(xy)$ of the Helmholtz wave equation with the condition given in (3). The first member has the following expression:

$$\phi^{(1)}(xy) = \gamma x\cos(\alpha x + \beta)\sin(\gamma y + \delta) - \alpha y\sin(\alpha x + \beta)\cos(\gamma y + \delta). \tag{5}$$

It is easily seen that these wave functions can be written as:

$$\begin{aligned}\phi^{(n)}(x,y) = {} & f_1(x,y)\sin(\alpha x + \beta)\sin(\gamma y + \delta) \\ & + f_2(x,y)\sin(\alpha x + \beta)\cos(\gamma y + \delta) \\ & + f_3(x,y)\cos(\alpha x + \beta)\sin(\gamma y + \delta) \\ & + f_4(x,y)\cos(\alpha x + \beta)\cos(\gamma y + \delta).\end{aligned} \tag{6}$$

Substitution in the Helmholtz wave equation gives us the following four coupled-differential equations for the functions $f_1(x,y)$, $f_2(x,y)$, $f_3(x,y)$, and $f_4(x,y)$:

$$\begin{aligned}\nabla^2 f_1(x,y) + 2\left(\gamma\frac{\partial f_2(x,y)}{\partial y} + \alpha\frac{\partial f_3(x,y)}{\partial x}\right) &= 0 \\ \nabla^2 f_2(x,y) + 2\left(\gamma\frac{\partial f_1(x,y)}{\partial y} - \alpha\frac{\partial f_3(x,y)}{\partial x}\right) &= 0 \\ \nabla^2 f_3(x,y) + 2\left(-\gamma\frac{\partial f_4(x,y)}{\partial y} + \alpha\frac{\partial f_1(x,y)}{\partial x}\right) &= 0 \\ \nabla^2 f_4(x,y) + 2\left(\gamma\frac{\partial f_3(x,y)}{\partial y} + \alpha\frac{\partial f_2(x,y)}{\partial x}\right) &= 0.\end{aligned} \tag{7}$$

We assume an air-filled hollow uniform waveguide with perfect conducting walls, according to the customary Dirichlet boundary condition, where $\phi^{(n)}(xy) = 0$ on the walls, this equation has to be solved. However, except for $n = 0$, where $\phi^{(0)}(xy)$ is the separable solution, none of the resulting patterns define closed areas. Linear combinations of $\phi^{(0)}(x,y)$ and $\phi^{(n)}(x,y)$ in the form of

$$\phi(x,y) = \phi^{(0)}(x,y) + \sum_n C_n\phi^{(n)}(x,y) \tag{8}$$

produce closed boundaries only when n is even.

By choosing appropriate values of the constant C_n, any shape between a square and a circle can be approximated as shown in Fig. 1. Moreover, we end up with an exact analytical expression. However, it turns out that there is a maximum value for the constant factors C_n, which when exceeded show no closed contours.

Let us now concentrate on the TM mode and a second-order combination of the wave function

$$\phi(x,y) = \phi^{(0)}(x,y) + C_2\phi^{(2)}(x,y). \tag{9}$$

Starting from a TM_{11} mode in a rectangular waveguide with dimensions a and b, the solution for the axial electric field E_z becomes

$$E_z = \sin x\sin\frac{\pi}{b}y + C_2 f(x,y,\pi,b) \tag{10}$$

with $f(x,y,\pi,b)$ the nonseparable solution of the second-order given by

$$\left[\left(\frac{\pi}{b}x\right)^2 + y^2\right]\sin x\sin\frac{\pi}{b}y + \frac{\pi}{b}y\sin x\cos\frac{\pi}{b}y + x\cos x\sin\frac{\pi}{b}y + 2x\frac{\pi}{b}y\cos x\cos\frac{\pi}{b}y \tag{11}$$

and $a = \pi$.

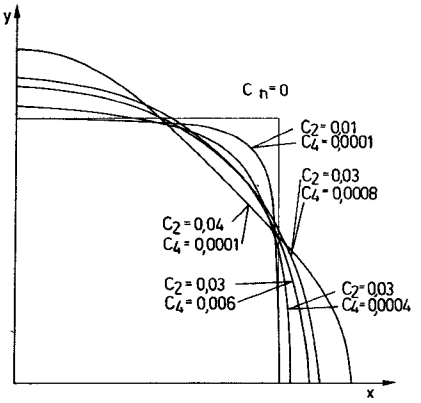

Fig. 1. Cross-sectional shapes resulting from $\phi^0(xy) + C_2\phi^2(xy) + C_4\phi^4(xy) = 0$.

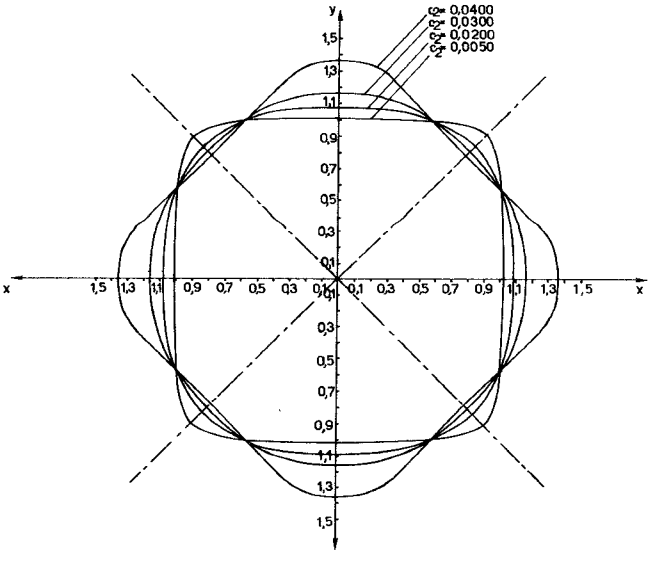

Fig. 2. Waveguide cross sections for various values of C_2.

Depending on C_2, various forms of cross sections can be found, as shown in Fig. 2.

A salient feature of the figure can be seen. For $C_2 < 0.01$, the second term in (10) is a small perturbation of the original separable solution, and results in a rectangular cross section with rounded corners.

For $C_2 > 0.01$ the cross section totally departs from the original rectangular shape. We actually have a maximum C_2 value in order to obtain closed boundaries.

Fig. 3 shows C_{max} against the dimensions a/b for combinations of $\phi^{(0)}(x,y)$ with a second- and fourth-order nonseparable solution. The second-order combination has a wide range of C_2 values resulting in a cross section with closed boundaries. Investigation of the cutoff frequency as a function of C_2 and with a/b as a parameter, presented in Fig. 4, shows a small increase in frequency. We note that these results are in agreement with those obtained in the study of rectangular cross sections with rounded corners [4]. So far we can conclude that nonseparable solutions can be used for describing TM modes in waveguides with general cross sections varying from square or rectangular shape with rounded corners to a form that has nothing in common with the original one.

Let us consider the field energy and power. The power in the axial direction of the waveguide is given by:

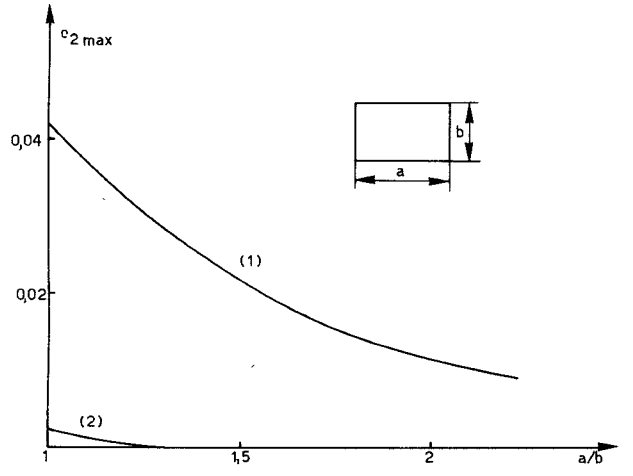

Fig. 3. Max C_2 against dimensions of rectangular waveguide. Curve (1) $\phi(x, y) = \phi^0 (xy) + C_2 \phi^2 (xy)$. Curve (2) $\phi(x, y) = \phi^0 (xy) + C_4 \phi^4 (xy)$.

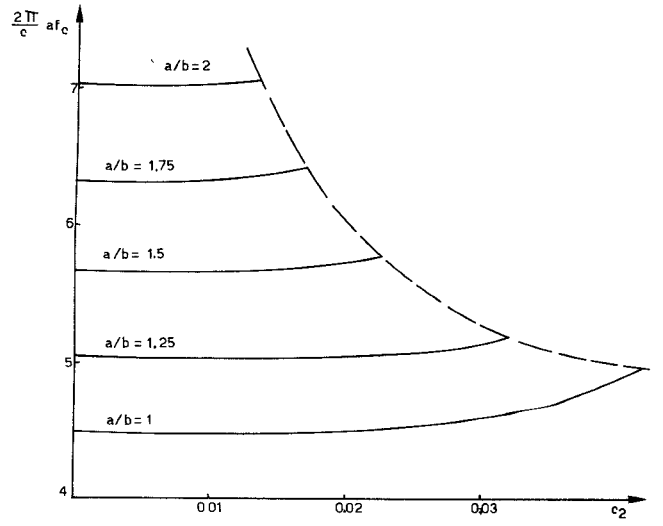

Fig. 4. Variation of cutoff frequency f_C as function of perturbation factor C_2.

$$P_z = \frac{1}{2}\frac{\beta^2}{k_c^2} Y_e \int_A E_z E_z^X \, dA \tag{12}$$

where A is the cross section of the waveguide and Y_e and β are the wave admittance and the propagation factor, respectively. Substitution of (10) in (12) leads to

$$P_z = \frac{1}{2}\frac{\beta^2}{k_c^2} Y_e \int_A \left[\sin^2 x \sin^2 \frac{\pi}{b} y + 2C_2 f(x,y,\pi,b) + C_2^2 f^2(x,y,\pi,b) \right] dA. \tag{13}$$

In order to compare waveguides of perturbed cross section with those of rectangular cross section, we define the relative power:

$$P_{rel} = \frac{P_z}{P_z'} \tag{14}$$

where P_z and P_z' are the powers of the perturbed and rectangular cross sections, respectively. After reduction to the same cross-sectional surface, Fig. 5 shows the relative power flow P_{rel} versus the perturbation factor C_2 with a/b as a parameter. At this stage we can conclude that, with respect to energy transport, a waveguide synthesized with nonseparable solutions can support more power depending on the value of C_2 and secondly that rectangular waveguides do not need accurately finished corners. Indeed, some rounded corners give a better energy transport. Investigation of the maximum amplitude of the electric field $|E_z|_{max}$ normalized to the maximum amplitude of the field in the rectangular cross section for constant relative power, as shown in Fig. 6, indicates that for constant power, values of $C_2 > 0.014$ result in an increasing value of $|E_z|_{max}$. However, high values of C_2 result in significant distortion of the original rectangular cross section and obviously are more diffi-

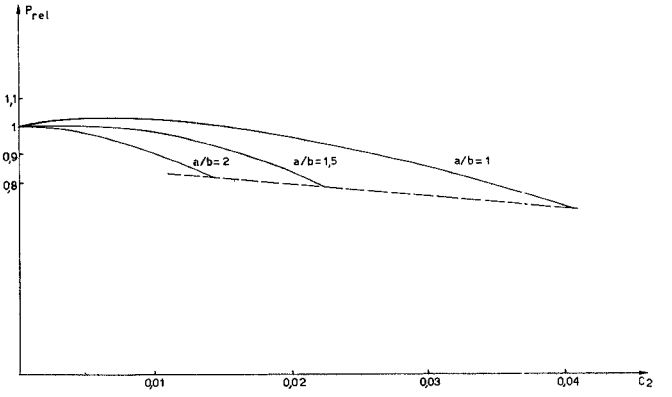

Fig. 5. Relative power flow P_{rel} versus the perturbation factor C_2 with a/b as a parameter and for normalized areas of cross sections and normalized amplitudes.

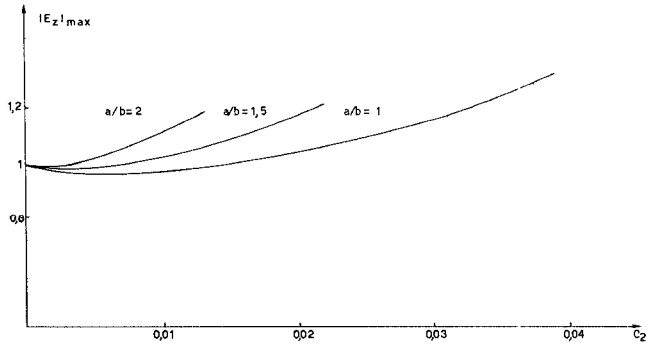

Fig. 6. $|E_z|_{max}$ versus C_2 with a/b as a parameter.

cult to construct. A very good compromise can be found for C_2 between $0.014 < C_2 < 0.04$. This results in $1.04 < |E_z|_{\max} < 1.36$.

Other important properties are the attenuation factor and the Q factor. Taking into account finite conductivity of the waveguide walls for a TM mode, the attenuation constant has the following expression:

$$\alpha = \frac{(C/2A)[(\epsilon_0/\mu_0)]^{1/2}R_m}{[1 - (\omega_c^2/\omega^2)]^{1/2}}\xi_c \tag{15}$$

where

- C circumference of the cross section;
- A area of the cross section;
- R_m surface resistance;
- ξ_c dimensionless number depending on the shape of the cross section and given by the following relation:

$$\oint_c \frac{1}{\omega_c^2}\left|\frac{\partial E_z}{\partial n}\right|^2 d1 = \xi_c\epsilon_0\mu_0\frac{C}{A}\int_A |E_z|^2\,dA. \tag{16}$$

The relative attenuation factor compares the attenuation in the perturbed waveguide by the use of nonseparable solutions, with that of the nonperturbed or rectangular waveguide and is given as follows:

$$\alpha_r = \frac{(C/2A)\xi_c}{(C'/2A')\xi_c'} = [(C/2A)]_r\xi_{cr}. \tag{17}$$

In Fig. 7 we show $(C/2A)_r$ and ξ_{cr} versus the perturbation factor C_2.

It is obvious that only the factor ξ_{cr} has a considerable variation and is therefore a measure of the attenuation factor presented in Fig. 8. For cylindrical cavities, the Q factor is given by:

$$Q = \frac{\mu}{\mu_c}\frac{d}{\delta}\frac{1}{2[1 + \xi_c(Cd/4A)]} \tag{18}$$

where

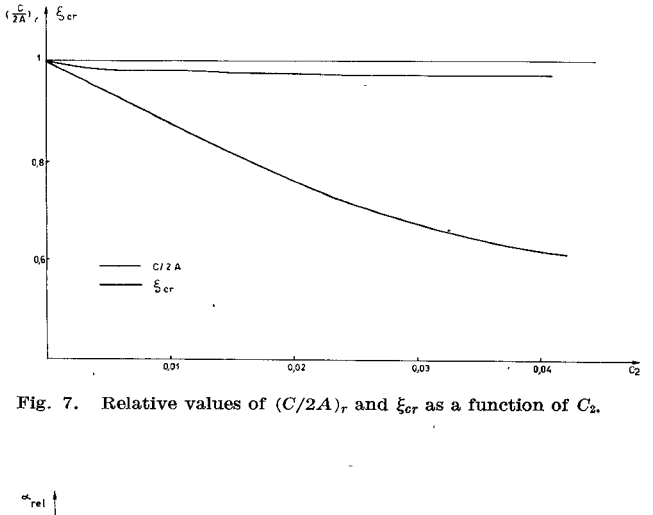

Fig. 7. Relative values of $(C/2A)_r$ and ξ_{cr} as a function of C_2.

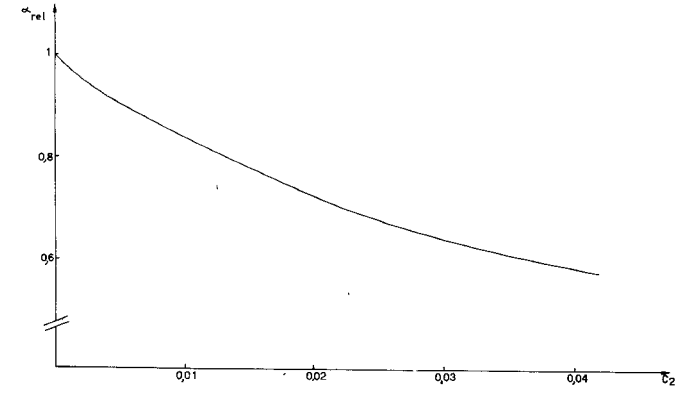

Fig. 8. Relative attenuation factor versus the perturbation factor C_2.

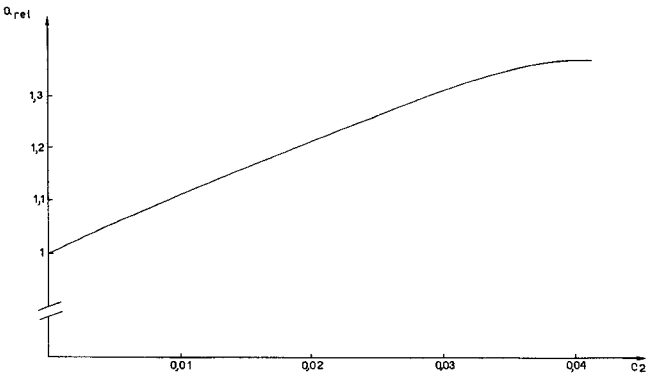

Fig. 9. Relative Q factor versus the perturbation factor C_2.

- u_c permeability of the metal walls of the cavity;
- δ skin depth;
- d length of the cavity.

In the same manner a relative Q factor can be defined in the form

$$Q_r = \frac{1 + \xi_c Cd/4A}{1 + \xi_c' C'd/4A'}. \tag{19}$$

Fig. 9 shows Q_r as an increasing function of the perturbation factor C_2.

In conclusion we can say that nonseparable solutions of the Helmholtz wave equation are suitable for describing TE and TM modes in waveguides and cavities with general cross sections; moreover, they are exact wave functions for any deformed conventional rectangular or circular waveguide so that no approximate method of solutions has to be taken. Further, it has been shown that waveguides and cavities synthesized with nonseparable solutions have better attenuation and higher Q factor than comparable conventional waveguides shapes.

Further, it is clear that they have interesting properties for microwave measurement and power applications. All calculations were done on the computer of the Rekencentrum of the Catholic University of Louvain.

REFERENCES

[1] P. M. Morse and H. Fesbach, *Methods of Theoretical Physics*. New York: McGraw-Hill, 1953, pp. 753–757.
[2] D. S. Moseley, "Nonseparable solutions of the Helmholtz wave equation," *Quart. Appl. Math.*, vol. 22, pp. 354–357, 1965.
[3] P. J. Luypaert and D. H. Schoonaert, in *1974 Proc. Microwave Power Symp.*, pp. B5-1/1–B5-1/3 and B5-4/1–B5-4/3.
[4] P. Lagasse and J. van Bladel, "Square and rectangular waveguides with rounded corners," *IEEE Trans. Microwave Theory Tech.*, vol. MTT-20, pp. 331–337, May 1972.

Tapered Asymmetric Microstrip Magic Tee

M. H. ARAIN AND N. W. SPENCER, MEMBER, IEEE

***Abstract*—The design, development, and constructuion of a very compact decade-(1–10-GHz) bandwidth microstrip −8.34-dB coupler are described. Calculations are given for the voltage coupling coefficient and the low-frequency cutoff, and the method of determing the physical dimensions of the circuit is described. Also, the feasibility of a decade-bandwidth microstrip magic tee by cascading two −8.34-dB couplers is demonstrated by comparing the actual and theoretical results of a coupler.**

Manuscript received April 21, 1975; revised August 26, 1975.
The authors are with the Autonetics Group, Rockwell International, Anaheim, Calif. 92803.